# Experimental investigations on a portable atmospheric water generator for maritime rescue

Du Runze, Ma Qingfen, Lu Hui, Wang Gaoping, Ye Wei, Cao Guangfu and Cui Yifan

## ABSTRACT

To offer an alternative for supplying fresh water to people in distress in tropical seas before rescue or to garrison soldiers on a small reef, a portable solar-photovoltaic atmospheric water generator was designed and tested experimentally, and is composed of a water generating module, a water purifying module, a power supply and control module, and a buoyancy module. The results showed that the best water production rate of 460 mL/h was achieved when $T_{in} = 27$, $RH_{in} = 92\%$, $Q_a = 600\ m^3/h$, with the desalination rate above 99.65%, proving itself a feasible solution as a portable desalination device. The daily water production can reach 5.52 L/d, which is more than twice the minimum quantity of the WHO drinking water standard (2.5 L/capita-day), and the energy consumption can be controlled under 200 W. The influences of major operating parameters on the device performance were analyzed and performance comparisons were carried out with the reported AWG products/prototypes. By integrating with a distress signal launcher and positioning module to shorten rescue time, the device has the potential to be employed as a small rescue platform for people in distress in tropical oceans, carried on board ship as a precaution.

**Key words** | atmospheric water generator, maritime search and rescue, portable seawater desalination, potable water supply

**Du Runze**
**Ma Qingfen** (corresponding author)
**Wang Gaoping**
**Ye Wei**
**Cao Guangfu**
**Cui Yifan**
College of Mechanical and Electrical Engineering,
Hainan University,
Haikou, Hainan 570228,
China
E-mail: *mqf0920@163.com*

**Lu Hui**
Chinese Academy of Tropical Agriculture Sciences,
Institute of Environment and Plant Protection,
Haikou, Hainan 571101,
China

## INTRODUCTION

Maritime safety has attracted increasing attention in recent years due to increasingly frequent maritime activities, such as sailing, deep-sea aquaculture, maritime exploration and development, etc. Maritime emergencies or accidents like collisions, grounding, and sinking occur more frequently, causing loss of crew life and great damage to the environment, the ship and carried cargo (Goerlandt & Montewka 2015; Fox *et al.* 2016; Størkersen *et al.* 2017). Maritime search and rescue (SAR) is one of the most effective ways to minimize such consequences by searching for missing persons at sea and finding lost objects like drifting containers or wrecks, and where, timeliness is one of the most essential issues, especially in human search missions. However, due to the complexity and broadness of the seas, the time to reach the position and then the rescue is an uncertainty indicating that the human in distress must wait an unpredictable period before they can be successfully rescued. In tropical oceans, such as the South China Sea, the temperature of the surface can be 25 °C–28 °C all year round, which is beneficial to maintain the vital signs and prolong the tolerance duration of life, compared with the temperate or frigid oceans, but the key barrier to survival is the provision of the necessary potable water supply. Portable seawater



doi: 10.2166/wrd.2020.048

desalination devices are a good solution in such cases, and should be able to generate potable water from seawater automatically, driven by renewable energy sources, float on the surface, be small in volume and light in weight.

Solar powered reverse osmosis (RO) systems are a promising technology for remote communities with water shortage by generating drinking water from brackish water (Freire-Gormaly & Bilton 2019b). These systems must face the challenge of premature membrane fouling caused by their intermittent operation due to the variation in the solar energy (Freire-Gormaly & Bilton 2017). Some experimental investigations have been carried out to reveal the impact of intermittent operation on membrane fouling and optimize the system (Freire-Gormaly & Bilton 2017, 2018, 2019a; Freire-Gormaly 2018). Although these systems can be designed for portable water production, there are still some challenges when they are applied for maritime rescue. For example, the increase in salinity of seawater compared to brackish water requires the adoption of a high-pressure pump and energy recovery device, leading to weight and volume increase, high requirement for operation, large area of solar panel, and so on.

The solar still is a very simple device for portable water production, especially as a suitable solution for fresh water issues in remote areas. It is simple in construction, operation and maintenance, and environmentally friendly, yet has the disadvantages of low productivity and large installation area requirement. Several methods were reported for the improvement of productivity and efficiency by integrating the still with sensible heat storage materials (Murugavel *et al.* 2010; Rajaseenivasan *et al.* 2013) and latent heat storage materials (Dashtban & Tabrizi 2011), coupling thermoelectric devices (Esfahani *et al.* 2011), flat plate collectors (Sheeba *et al.* 2015) and reflectors (Omara *et al.* 2017), employing the configuration of triangular pyramid (Nagarajan *et al.* 2014; Sathyamurthy *et al.* 2014), pyramid (Kabeel *et al.* 2017), hemisphere (Arunkumar *et al.* 2012) and tubes (Singh & Tiwari 2017), separating condensers (Madhlopa & Johnstone 2009), and developing multiple-effect stills (Abdessemed *et al.* 2019) and sun tracking devices (Mutasher *et al.* 2010), etc. However, only a few studies have focused on the portable solar still.

Wassouf *et al.* (2011) designed, constructed, and tested two novel prototypes of portable solar stills, i.e., a 0.2 $m^2$ pyramidal polyvinyl chloride (PVC) and a 0.6 $m^2$ triangular-prism PVC solar still. Based on the parameter analysis, configuration designs, manufacture technique, and the material selections, the solar stills were constructed. The test results showed that the stills generated an average of 0.5 L/day and 0.9 L/day of distilled water, respectively, with turbidity levels not exceeding 3 NTU. Esfahani *et al.* (2011) applied thermoelectric cooling in a portable active solar still and performed experimental tests under the climate condition of Semnan, Iran, on winter days. Being an active solar still, a 12 V power source was chosen for driving the pump, fan, and thermoelectric cooler (TEC1-12706). The results showed that the ambient temperature and solar radiation had a positive effect on water generation and wind speed had a negative effect on water productivity. By integrating the thermoelectric cooler, the performance was effectively improved, approaching that of the conventional one operated in summer. The maximum hourly and 7-hour accumulative water production rates were about 250 mL/$m^2$ and 1,700 mL/$m^2$, respectively. The cost analysis was carried out without the discussion of specific energy consumption. Rahbar & Esfahani (2012) experimentally studied a novel solar still integrated with a heat pipe and thermoelectric module. The solar intensity, wind velocity, ambient temperature, water production, temperature of thermoelectric module and heat pipe were measured, obtaining similar factor effects to the tests of Esfahani *et al.* (2011). A thermoelectric module TEC1-12708, which was cooled by a commercial heat pipe 'CoolerMaster hyper Z600R', together with a fan, was mounted in the roof region to cool an aluminum plate for condensation. The maximum hourly and 7-hour accumulative water production rate was only about 160 mL/$m^2$ and 885 mL/$m^2$, respectively, even on a typical summer day, and the energy consumption of the system was not mentioned either. Later, Rahbar *et al.* (2016) continued to study the solar still integrated with thermoelectric modules, and proposed and tested an asymmetrical solar still. The minimum and maximum daily productivity was about 225 and 500 mL in the solar intensity of 20,500 and 25,500 J/$m^2$, respectively. Derived from their experimental results, the energy consumption of the thermoelectric modules (TEC-12708) and fans were about 233 W and the hourly water productivity was about 62.5 mL. Sathyamurthy *et al.* (2015) designed, fabricated, and tested a portable solar still with

evaporation and condensation chambers in summer conditions. The solar still consisted of an evaporating chamber, a condensing chamber and phase change material (PCM) in between them for heat recovery from solar intensity as well as the latent heat. Due to the stored energy in the PCM, the water production period lasted much longer than the solar still without PCM, leading to a remarkable improvement of the accumulated yield from 1.05 L/day to 1.6 L/day, an increase of 52%.

An atmospheric water generator produces fresh water by condensing the vapor in the air by virtue of cooling cycles or thermoelectric coolers (TECs). Compression refrigeration cycles and absorption refrigeration cycles are two well-known cooling cycles used in AWG (Anbarasu & Pavithra 2011; Praene *et al.* 2011; Kabeel *et al.* 2016; Alobaid *et al.* 2017; Farhad *et al.* 2018; Li *et al.* 2018) and have also been employed in some portable devices. Anbarasu & Pavithra (2011) proposed a portable AWG generating fresh water by a vapor compression refrigeration system equipped with a 1.1 kW compressor. It was reported that the average water productivity was 763 mL per hour at an average of 70% *RH* (relative humidity), with higher efficiency than other refrigeration systems. Niewenhuis *et al.* (2012) proposed a dehumidifier with liquid desiccant method and the water productivity was only 72.1 mL per kW-hr.

In recent decades, AWGs with TECs have attracted much attention since TECs are very small, quiet, maintenance-free, and reliable electronic devices with no need for any other refrigerant gases. However, due to the low efficiency of TECs, the water productivities were not sufficient to meet the demand for a portable water generator. Vián *et al.* (2002) proposed and tested a two-stage thermoelectric dehumidifier equipped with three TECs and two axial fans. The energy consumption of TECs was about 180 W and the condensed water flow rate was 0.969 L/day. Yıldırım *et al.* (2014) carried out an experimental investigation of a portable desalination unit configured by a single TEC module, TEC1-12709. The maximum daily yield of the system and the coefficient of performance (COP) of the thermoelectric cooler were reported as 143.6 g and 0.78, respectively. Pontious *et al.* (2016) developed two AWG concepts, one utilizing a heat exchanger with the coolant cooled at a lower ground temperature, the other one utilizing the Peltier thermoelectric coolers. They also designed and tested two prototypes, with energy requirement of 31.8 W and 22.2 W, respectively. The two prototypes were tested under different relative humidities; using heat exchange could obtain a hourly water productivity of 41.2 mL while using the thermoelectric coolers could only obtain 5.1 mL. Liu *et al.* (2017) performed experimental analysis of a portable AWG by thermoelectric cooling method. The influences of relative humidity of inlet air and air flow rates were investigated and the maximum water productivity was 25.1 g/h with input power of 58.2 W. Joshi *et al.* (2017) designed and tested a prototype of the thermoelectric fresh water generator consisting of a cooling channel along with ten thermoelectric modules. An internal heat sink was placed on the cold side of the modules to enhance heat transfer rate. After operating for 10 hours, the maximum water condensate obtained using internal heat sink was 240 mL which was 5.3 times of that without internal heat sink.

Since the portable solar still occupies a larger land area and the AWG with absorption refrigeration cycles or thermoelectric cooler had limited water productivities, we designed a portable solar-PV AWG (PS-AWG) with compression refrigeration cycles and lower energy consumption for the purpose of supplying fresh water for people in distress in tropical oceans before rescue or for garrison soldiers on a small reef. The PS-AWG can be integrated with a distress signal launcher and positioning module to shorten rescue time. In this paper, the design of the AWG device and its modules are presented next, followed by introduction of the experimental apparatus and parameters, and then the testing results are analyzed and discussed.

## DESIGN OF AWG AND ITS MODULES

The AWG generates fresh water from moist air based on the principle of the humidification-dehumidification (HDH) process in which the water evaporator and condenser are necessary components. For the purpose of sea rescue, the designed AWG will be placed to float upon the surface of the tropical sea where water is evaporated continuously under the sunshine. Thus, a layer of moist air with *RH* approaching 100% is generated near the sea, forming a 'natural water evaporator' for AWG. Figure 1 shows the working principle of the proposed AWG. The 'natural

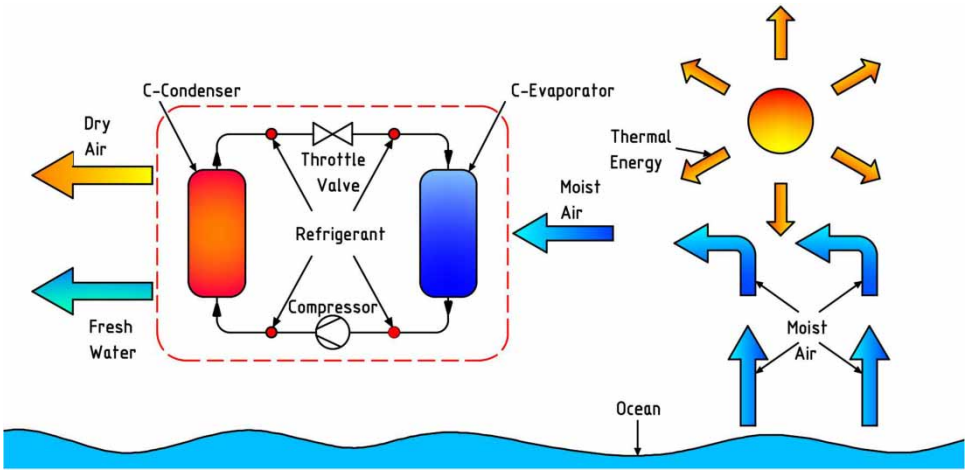


**Figure 1** | Working principle of the AWG.

water evaporator' and the compression refrigeration cycle are employed to humidify and dehumidify the air, respectively, to obtain fresh water from moist air. A type of common and friendly environmental coolant is chosen as the medium of the refrigeration cycle which is composed of a coolant evaporator C-Evaporator, a coolant condenser C-Condenser, a compressor, and a throttle valve. Figure 2 shows the schematic diagram of the proposed AWG device. It is composed of a water generating module, a water purifying module, a power supply and control module, and a buoyancy module.

## Water generating module

The water generating module is designed to desalinate the tropical seawater with the maximum salinity of 35‰.

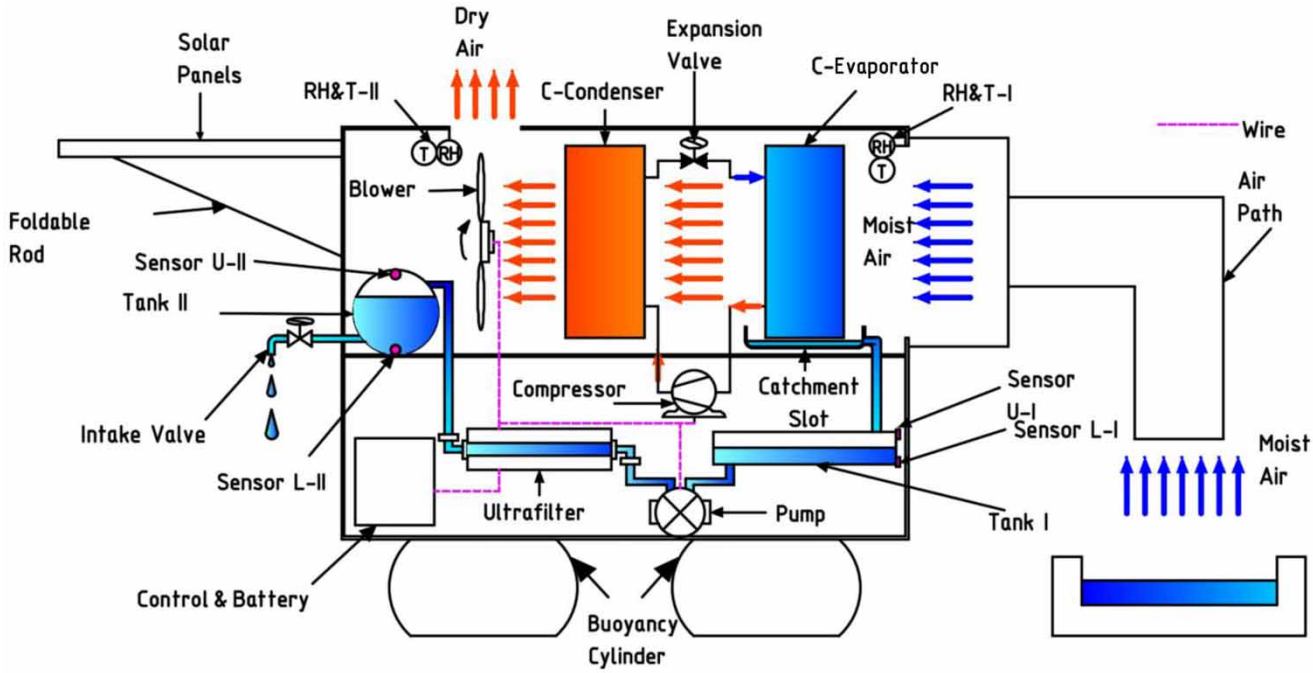


**Figure 2** | Schematic diagram of the proposed AWG device.

The water generating module includes an air path, a compression refrigeration cycle, a catchment slot, and a blower. Driven by the blower, the moist air from the sea's surface is sucked into the device though the air path, cooled by the coolant evaporator (C-Evaporator) with condensed water collected into the catchment slot, then warmed by the heat from the coolant condenser (C-Condenser) and the compressor, and finally discharged from the air outlet. The air flow rate can be adjusted by the blower speed to control the absolute water content of the sucked moist air and the temperature in the device.

## Water purifying module

The water purifying module is made up of a primary water tank (Tank I), a pump, an ultrafilter, a secondary water tank (Tank II), and an intake valve. The condensed water in the catchment slot automatically flows into the primary water tank under gravity, then is pumped to the secondary water tank through the ultrafilter to remove the impurities, and finally can be used when turning on the intake valve.

## Power supply and control module

The consumed power of the compressor, the pump, and the blower is converted from solar energy by solar PV panels. Lithium batteries are adopted to store the converted electrical energy for their advantages of high storage energy density, long service life, low self-discharge rate, and light weight, etc. A DC-AC converter may be necessary when the AC is required for the power consumer.

The control module is designed to collect data from sensors and switch the operation mode of the AWG device. *RH* and temperature sensors are placed near the inlet and the outlet of air flow, respectively (*RH*&*T*-I and *RH*&*T*-II), and based on the tested data the absolute water content of air flow and the water removal rate can be calculated. Several sensors of liquid levels are placed in the upper limit and lower limit position of the primary water tank (U-I and L-I) and secondary water tank (U-II and L-II). A battery power detector (PD) is connected to the lithium batteries to detect relative state of charge and to alert when charge has dropped below a certain percentage. Based on the signals from liquid level sensors and the battery power detectors, the operating modes of the power consumers in the device can be controlled according to the strategy shown in Table 1. The number '1' and '0' represent 'True' and 'False' respectively. When the output signal of PD is '1', the battery power is larger than 15% of the capacity. The output signal of the sensor of liquid level equals to '1', indicating that the liquid level reaches where the sensor is located.

## Buoyancy module

The buoyancy module is mounted below the device, so that the device can float on the sea surface and enough distance between the water intake and the sea surface can be maintained facilitating the utilization of potable water. The

**Table 1** | Control strategy of the control module

| Output signal | | | | | | | |
|---|---|---|---|---|---|---|---|
| **PD** | **U-II** | **U-I** | **L-II** | **L-I** | **State description** | **Operating equipment** | **Operation** |
| 0 | 1/0 | 1/0 | 1/0 | 1/0 | The battery power is not enough | None | Charge batteries |
| 1 | 1 | 1 | 1 | 1 | The battery power is enough; Both water tanks are full | None | None |
| 1 | 1 | 0 | 1 | 1/0 | The battery power is enough; Tank II is full; Tank I is not full | Compressor blower | Generate water |
| 1 | 0 | 1/0 | 1/0 | 1 | The battery power is enough; Tank II is not full; Tank I is not empty | Compressor blower; Pump | Generate and pump water |
| 1 | 0 | 1/0 | 1/0 | 0 | The battery power is enough; Tank II is not full; Tank I is empty | Compressor blower | Generate water |

heavy parts, such as the batteries, the water tanks, and the compressor are mounted at the bottom of the device in order to lower the gravity center and keep the device upright even under the action and impact of waves.

## EXPERIMENTAL APPARATUS AND TESTING PARAMETERS

### Experimental apparatus

The prototype of the proposed AWG was designed, integrating the above modules together. Figures 3 and 4 show the 3-D model and photographs of the prototype. We made a prototype with a height of 1 m, a length of 0.8 m, and a width of 0.6 m. The shell, made up of ABS plates, is in cuboid configuration with side and top openings. The air path made of a retractable aluminum cylinder is connected to the side opening with the other end downwards close to the sea's surface. The inner space of the shell is divided into two sections, the top and the bottom section. All the power consumers, as well as heavy parts such as the compressor, the pump, the batteries, and the control hardware are arranged in the bottom section, all the wall seams of which are glued or sealed to cut off seawater. In addition, the primary water tank is placed in the bottom

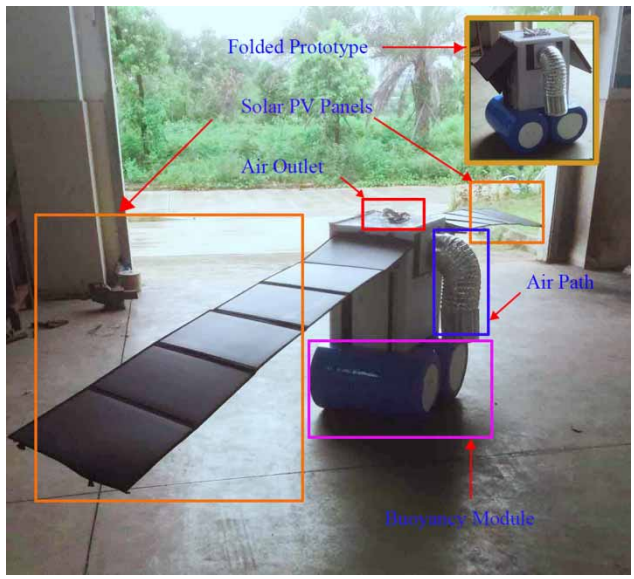


**Figure 4** | Photographs of the prototype.

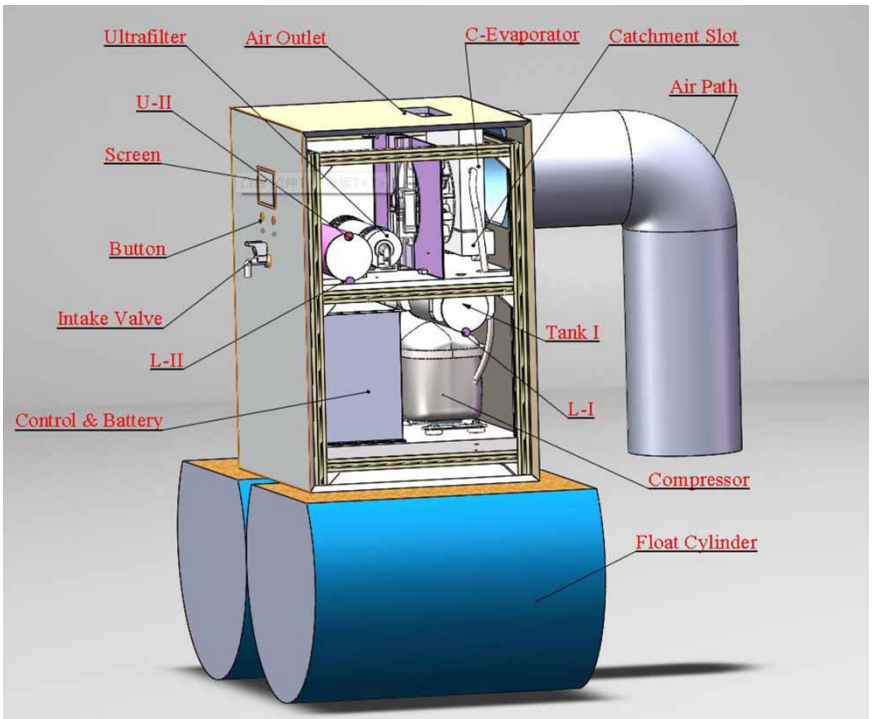


**Figure 3** | 3-D model of the prototype.

section to facilitate water fall from the catchment slot. In the top section, the C-Evaporator and C-Condenser made of copper tubes, as well as the blower, catchment slot, the ultrafilter, and the intake valve are mounted. A connection hole between the two sections is made for pipes and wires and sealed to prevent water entering into the bottom section. A small opening is made on the top of each water tank, and all the openings as well as the top of the catchment slot are covered with a layer of waterproof film to prevent water entering and to balance the pressure. Buoyancy cylinders are mounted below the device to keep the bottom of the device away from seawater.

The power supply system includes two foldable solar PV panels (150 W each) and two 12 V 100 Ah lithium batteries. The foldable solar PV panels are mounted on the two side walls, respectively, that are spread when operating at sea but folded on board to save space. The batteries should be fully charged on board to ensure the device can be operated immediately once an accident happens. During the operation, the solar PV panels can supplement the power consumption gradually. All the power consumers operate under voltage of 12 V, and the rate power of the compressor, the pump, and the blower are 196 W, 8 W, and 40 W, respectively. The actual power of the blower varies when its speed is adjusted by a frequency converter. Two *RH* and temperature sensors SHT30 are mounted near the inlet and outlet of the air flow. Four non-contact liquid level sensors are mounted outside of the primary and secondary water tanks, on the side wall. STM32F1 chips were embedded to develop a control module based on μC/OS-III real-time operating system which was connected to the peripheral resistive screen through the IIC protocol to display the detected parameters.

The performance of the AWG was tested in the laboratory. A water bath was placed below and close to the downward end of the air path to generate moist air, playing the role of the 'natural water evaporator'. The NaCl solution was adopted to simply simulate the seawater. The ambient temperature in the laboratory was maintained at 25 °C–30 °C, approaching the actual environmental temperature of the device.

## Testing parameters and sensors

To investigate the performance of the device, some parameters were tested directly, such as relative humidity (*RH*, %), temperature (*T*, °C) and volume flow rate ($Q_a$, $m^3/h$) of air flow, water production rate ($Q_w$, mL/h), and electrical conductivity ($\sigma$, $\mu$S/cm) of NaCl solution and water product, based on which, other parameters were derived including the absolute water content of the sucked moist air, i.e., the water vapor flow rate at inlet ($Q_{wt}$, mL/h), the condensing ratio (*CR*, %), and the energy conversion coefficient (*ECC*). All the parameters are listed in Table 2 and the necessary formulae are given for the derived parameters. The subscript 'in' represents the inlet state, and 'w' and 'v' the liquid water and vapor, respectively. $p_s$ and $p_a$ represent the saturated vapor pressure of water at airflow inlet and the ambient pressure, respectively, $h$ the latent heat of water, $w_{tot}$ the total power input of the device, $\alpha$ the water to air molar ratio, and $t_g$ the time of generating water per day. Condensing ratio (*CR*) means water productivity per hour compared to the ideal of water vapor that incoming air flow can hold per hour by the system. Production ratio (*PR*) means daily water productivity compared to the minimum quantity of WHO drinking water standard (2.5 L/capita-day).

Sensors used to measure the direct parameters mentioned above are shown in Figure 5. Relative humidity and temperature were measured by highly accurate Humidity & Temperature (R&H) sensors. The testing temperature range is −20 °C–70 °C and the precision is ±0.3 °C. The testing relative humidity range is 0–100% *RH* and the precision

**Table 2** | List of testing parameters

| Directly tested parameter | Derived parameter and formula |
|---|---|
| Relative humidity *RH*, % | Water vapor flow rate at inlet $Q_{wt} = \frac{1000 p_s Q_a RH_{in} \alpha}{p_a}$, mL/h |
| Temperature *T*, °C | Condensing ratio $CR = \frac{\rho_w Q_w}{\rho_v Q_{wt}} \times 100\%$, % |
| Water to air molar ratio $\alpha$ | Production ratio $PR = \frac{Q_w t_g}{2500}$ |
| Air flow rate $Q_a$, $m^3/h$ | Energy conversion coefficient $ECC = \frac{\rho_w Q_w h}{w_{tot}}$ |
| Water production rate $Q_w$, mL/h | |
| Electrical conductivity $\sigma$, μS/cm | |
| Salinity of feed water *S*, g/L | |

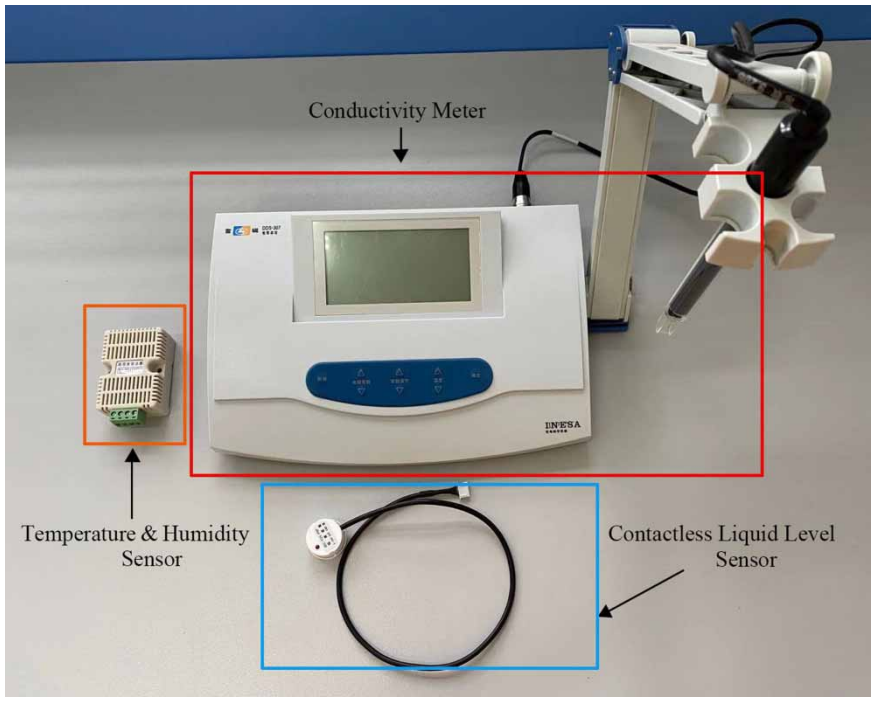


**Figure 5** | Testing sensors.

is 0.1 *RH*. The conductivity meter DDS-307 was used for testing the salinity of NaCl solution. The testing ability is 10–100.0 μS/cm and precision is ±1.5% (FS). Four contactless liquid level gauges were mounted on the limit positions of Tank I and Tank II to test the required liquid level.

## RESULTS AND DISCUSSION

### Feasibility analysis

To avoid the unnecessary errors and the uncertainties caused by the operation and variation of the surroundings and ensure the reliability of the reported value, all the tests were repeated at least three times, based on which variance analyses were carried out and shown in the related figures. Meanwhile, the relative deviations of the direct tested parameters were calculated, with the maximum value under 8%. Specifically, the relative deviation of $Q_w$, $T$, and $RH$ are 2.8%–4.3%, 0.7%–1.5%, and 3.5%–4.5%, respectively.

Eight-hour continuous tests were carried out to investigate the feasibility of the AWG device, and the testing results are shown in Figure 6. The device can realize the function of generating water from moist air, running almost stably with the best production rate of 460 mL/h when $T_{in} = 27\ ^{\circ}C$, $RH_{in} = 92\%$, $Q_a = 600\ m^3/h$. For each case, the water production rates of the first hour were all a bit larger than that of the later hours, indicating that the device experienced a 'start-up' phase before it can run

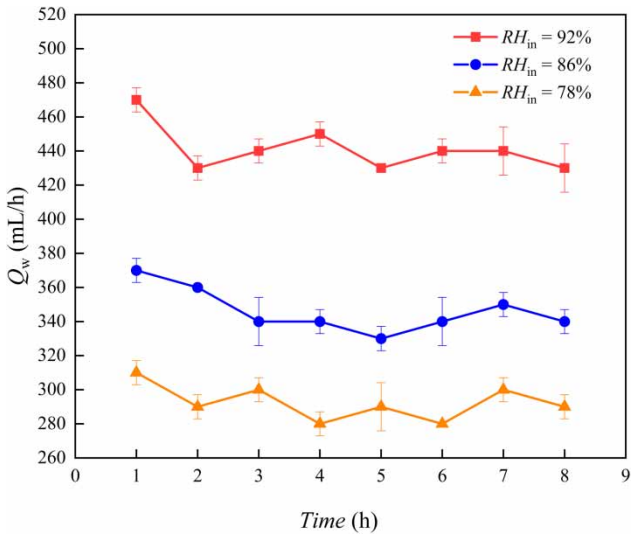


**Figure 6** | Water production rate of 8-hour continuous tests.

stably. Figure 7 compares the variation of the temperature in the device ($T_{de}$) and the temperature of airflow at inlet ($T_{in}$) during the first hour. A difference of 1 °C–2 °C between $T_{de}$ and $T_{in}$ was detected. When $T_{in}$ fluctuated around 25 °C, $T_{de}$ increased with the time yet the increase speed gradually slowed down, indicating that a thermal balance was being formed between the heat generated from power consumers and C-Condenser and the heat carried away with air flow.

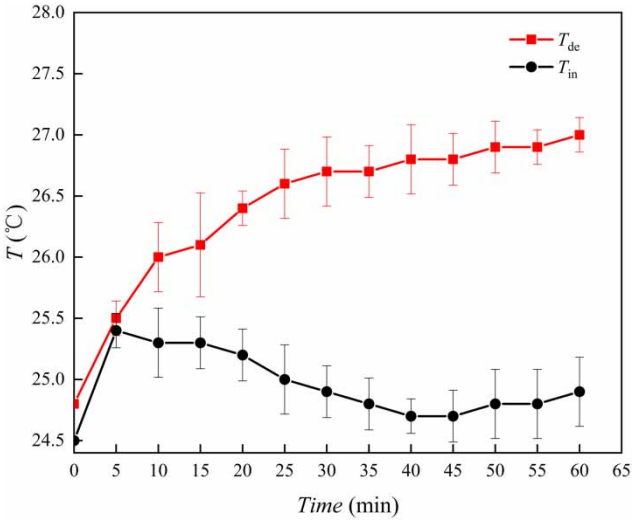


**Figure 7** | Variation of the temperature in the device $T_{de}$ and the temperature of air flow at inlet $T_{in}$ during the first hour.

Once the thermal balance formed, the water production rate can maintain stability thereafter.

To investigate the desalination rate of the device, six NaCl solutions with different concentrations were employed as the feed water. Figure 8 shows the electrical conductivity of the feed NaCl solution and the water product (DS represent distilled water), in which the $\sigma_f$, $\sigma_p$, $\sigma_d$, and $\Delta\sigma$ represent the electrical conductivity of feed solution, water product and distillated water, and the desalination rate, respectively. The desalination rates of the device are all above 99.65% and the salinities of water products are close to the distillated water, proving that the device can be effectively applied for seawater desalination. Also, since the ultrafilter was integrated in the device, the possible impurities in the condensation can be removed so that the water that flows out of the intake valve is potable. Thus, this device can supply a certain amount of potable water, proving itself an option for a portable desalination device.

## PERFORMANCE ANALYSIS

In this section, the influences of major operating parameters including the airflow temperature at the airflow inlet ($T_{in}$), relative humidity at the airflow inlet ($RH_{in}$), the air flow

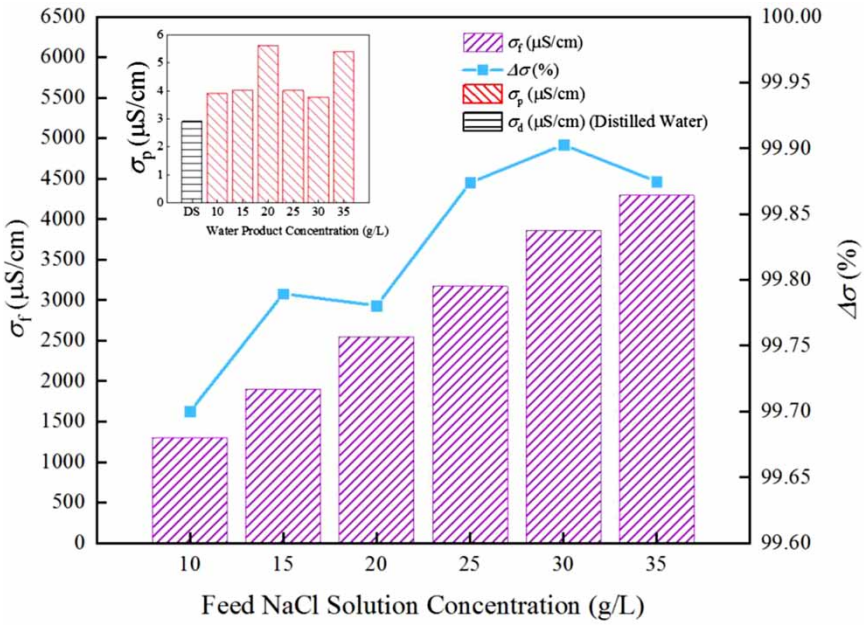


**Figure 8** | Electrical conductivity of the feed NaCl solution and the water product.

rate $Q_a$, and the salinity of the feed water ($S$) on the device performance will be discussed. The device performance can be chiefly measured by the water production rate, energy conversion coefficient, and condensing efficiency of vapor. Water production rate is always the first consideration when measuring the performance of a portable device. In some literature, the condensing ratio of vapor was considered as the second important measurement of the performance. However, for a portable desalination device applied on the sea, the energy efficiency should be considered prior to the condensing ratio.

## Influences of the temperature and relative humidity of air flow at inlet

Figure 9 shows the variation of water production rate ($Q_w$) with the temperature of air flow at inlet ($T_{in}$). When $RH_{in}$ is stabilized around 93%, with the increase of $T_{in}$, $Q_w$ increases until $T_{in}$ reaches 28.2 °C and then decreases. Although $Q_{wt}$ (water vapor flow rate at inlet) increases with $T_{in}$ given $RH_{in}$ a constant, the increase of $T_{in}$ will also cause the increase of the temperature in the device $T_{de}$ which has negative effect on the water condensation. Figure 10 shows the variation of the energy conversion coefficient $ECC$ and the condensing ratio $CR$ with the temperature of airflow at inlet $T_{in}$; higher energy conversion coefficient $ECC$ can be obtained by improving $T_{in}$ due to the increase of the absolute water content in the air flow. However, $T_{in}$ should not be improved all the time. Once it goes beyond a certain range, the condensing rate drops down sharply, leading to a remarkable decrease of the energy conversion coefficient even with increase of the absolute water content in the air flow. Thus, for a certain air flow rate, there is an optimal $T_{in}$, and its value will increase with the air flow rate.

Figures 10 and 11 show the variation of water production rate $Q_w$, the energy conversion coefficient $ECC$, and the condensing ratio $CR$ with the relative humidity at the inlet of airflow $RH_{in}$, respectively. When $T_{in}$ is stabilized around 26 °C, $Q_w$ and $ECC$ both increase with $RH_{in}$ due to the increase of the water vapor flow rate at inlet $Q_{wt}$, but the growth trend slows down gradually as the condensing ratio $CR$ cannot continuously increase, even decreasing after a certain value of $RH_{in}$.

## Influence of the air flow rate

Figures 12–14 show the variation of water production rate $Q_w$, the energy conversion coefficient $ECC$, and the condensing rate $CR$ with the air flow rate $Q_a$, respectively. Under the testing range, the increase of $Q_a$ has a positive effect on $Q_w$ and $ECC$, but the effect becomes weaker. When $Q_a$ increases from 360 $m^3$/h to 480 $m^3$/h, both the water vapor flow rate at inlet $Q_{wt}$ and the condensing rate $CR$ increase, leading to a remarkable rise of the water

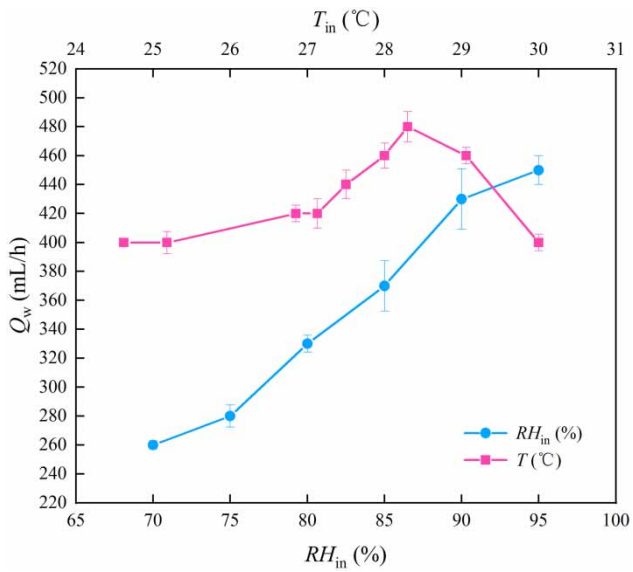


**Figure 9** | Variation of water production rate $Q_w$ with the temperature and relative humidity of air flow at inlet $T_{in}$ and $RH_{in}$.

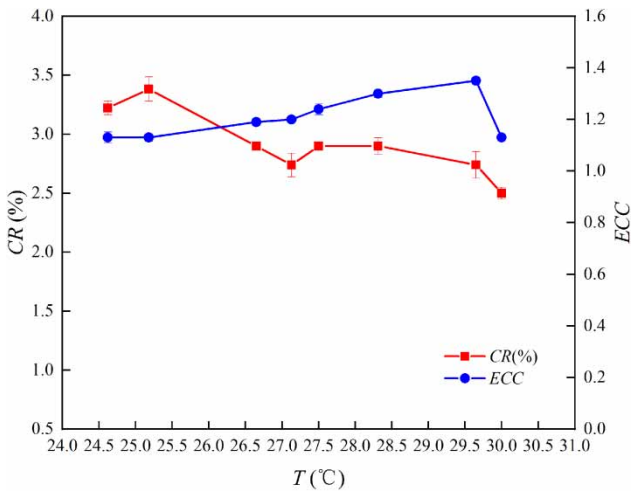


**Figure 10** | Variation of the energy conversion coefficient $ECC$ and the condensing ratio $CR$ with the temperature of air flow at inlet $T_{in}$.

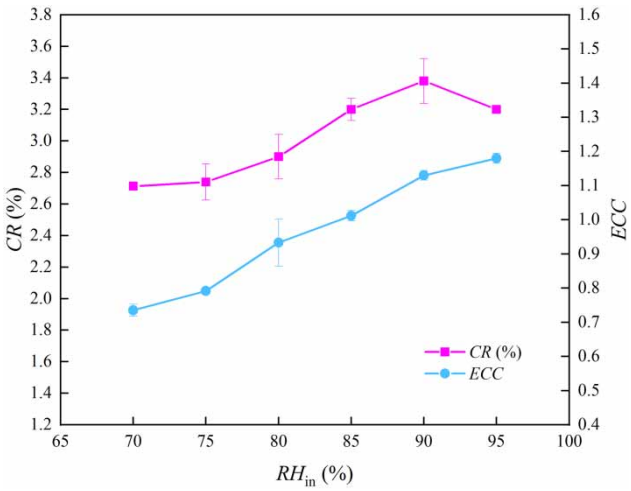


**Figure 11** | Variation of the energy conversion coefficient *ECC* and the condensing ratio *CR* with the relative humidity of air flow at inlet $RH_{in}$.

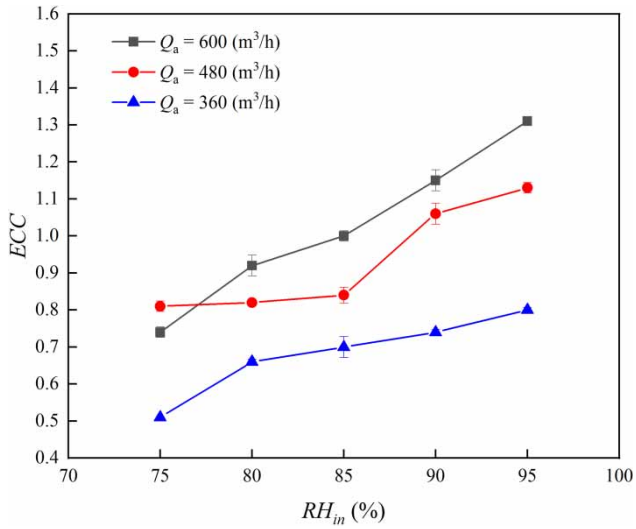


**Figure 13** | Variation of the energy conversion coefficient *ECC* with the air flow rate $Q_a$.

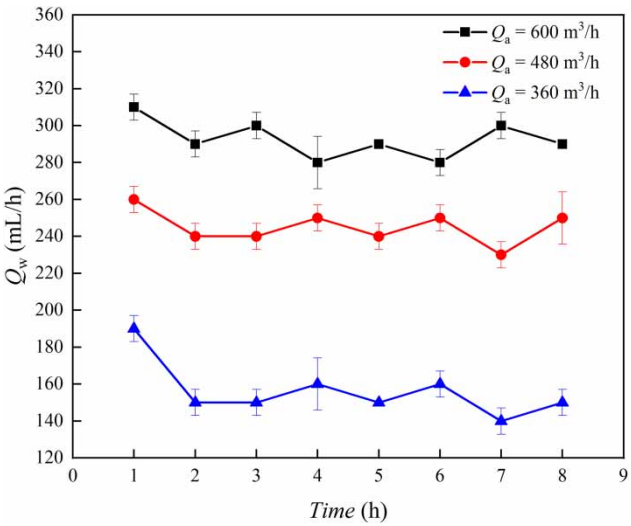


**Figure 12** | Variation of the water production rate $Q_w$ with the air flow rate $Q_a$.

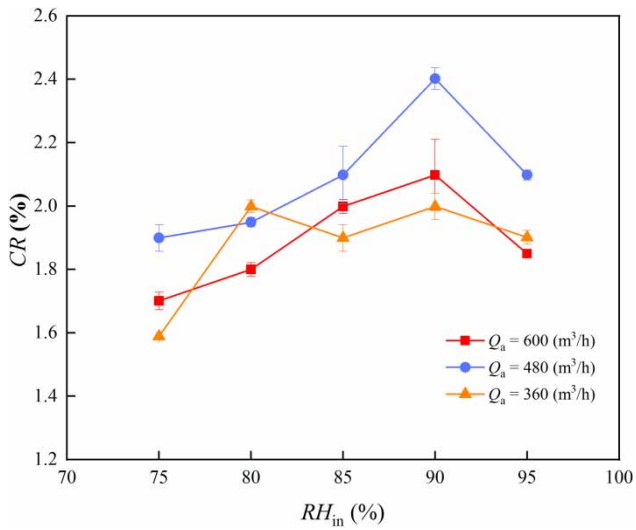


**Figure 14** | Variation of the condensing ratio *CR* with the air flow rate $Q_a$.

production rate $Q_w$ and the energy conversion coefficient *ECC*. When $Q_a$ increases from 480 $m^3/h$ to 600 $m^3/h$, although the water vapor flow rate at inlet $Q_{wt}$ increases, the condensing rate *CR* decreases, slowing down the rise of the water production rate $Q_w$ and the energy conversion coefficient *ECC*.

## Influence of salinity of feed water

Figures 15 and 16 show the influence of salinity of feed water *S* on the water production rate $Q_w$, the energy conversion coefficient *ECC*, and the condensing ratio *CR*. Although the water production rate $Q_w$ is a bit larger when the water bath is filled with distillated water, the difference caused by salinity variation is extremely small. Similarly, the salinity of feed water *S* can hardly influence the energy conversion coefficient *ECC* and the condensing ratio *CR*. Thus, salinity of the feed water *S* has little effect on the water production rate, the energy consumption, and quality of the water product, indicating that salinity of the sea area is not a consideration for the application of the device.

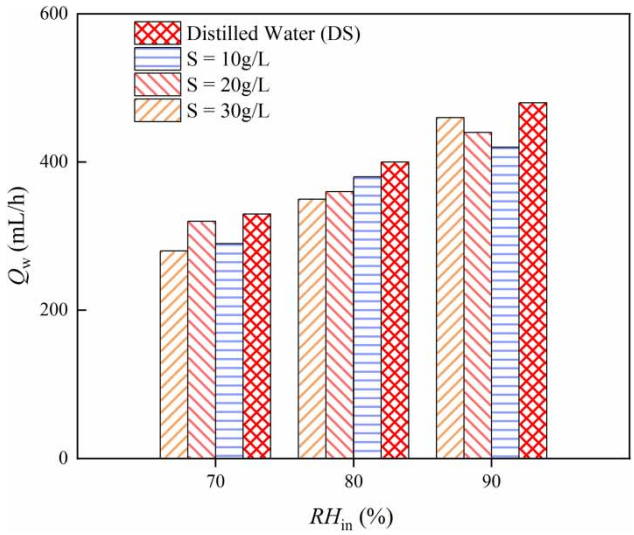


**Figure 15** | Influence of salinity of feed water $S$ on the water production rate $Q_w$.

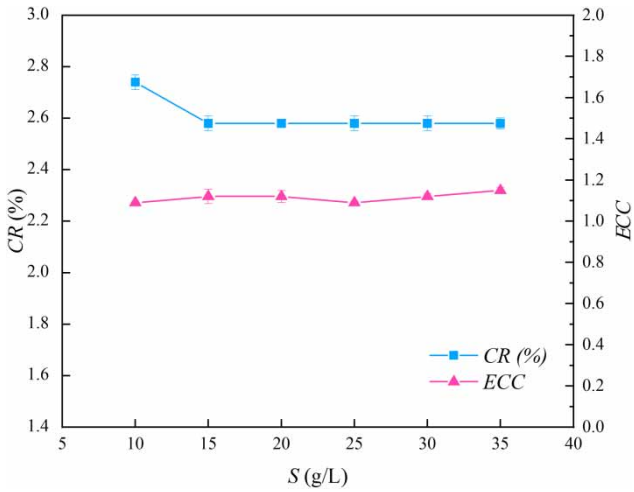


**Figure 16** | Influence of salinity of feed water $S$ on the energy conversion coefficient ECC and the condensing ratio $CR$.

## Performance comparisons

Performance comparisons of different AWGs are shown in Table 3. The experimental prototype in this study (shown as superscript ★ in the table) performed well for its higher water production rate and less *ECC* (both are key parameters for performance measurement, emphasized in bold in Table 3). The device is equipped with solar panels and lithium batteries as the energy supply system and will be applied in the tropical ocean where the sunshine duration can achieve 10 hours on a cloudless day. Thus, the maximum operation time can go beyond 12 hours, with maximum daily water production rate of 5.52 L/d. *PR* is equal to around 2.21, meaning that the daily water production rate is more than twice that of the WHO drinking water standard.

*CR* is equal to 2.9 meaning that only 2.9% mass of water vapor can be condensed compared to the total mass of water vapor that enters the system within an hour. Large air flow rate and insufficient cooling of the compressor were the main reasons for low condensation efficiency. For the high ambient temperature of the device, the heat generated from power consumers, especially the compressor, will improve the temperature in the device to an extent that is not favorable for water condensation and the operation of the compressor. Thus, a larger air flow rate is required to not only provide the vapor necessary for condensation but also take away the generated heat, directly leading to the lower condensation efficiency.

In view of this, the device should be improved further by designing a separate cooling system for the compressor which is independent of the air flow. An extra section can be designed below the bottom section of the device, in which the compressor is mounted separately. This extra

**Table 3** | Performance comparison of the AWG products/prototypes available and the proposed AWG

| | Operating parameters | | | | Performance evaluation | | |
|---|---|---|---|---|---|---|---|
| **Data source** | **$T_{in}$ (°C)** | **$RH_{in}$ (%)** | **$Q_a$ (m³/h)** | **$W_{tot}$ (W)** | **$Q_w$ (mL/h)** | ***ECC*** | ***CR* (%)** |
| 1 Kabeel *et al.* (2017) | 24.29 | 67.8 | 29.7 | 52.3 | **11.2** | **0.15** | 2.42 |
| 2 Madhlopa & Johnstone (2009) | 25.3 | 60.0 | 129.1 | 65.5 | **27.9** | **0.29** | 1.78 |
| 3 Abdessemed *et al.* (2019) | 27 | 82.0 | 13.68 | 100 | **40.3** | **0.27** | 13.62 |
| 4 Mutasher *et al.* (2010) | 30 | 65.0 | 80.3 | 135.0 | **5.0** | **0.02** | 0.31 |
| 5 Arunkumar *et al.* (2012) | 32 | 39.5 | 57 | 1,000 | **597.4** | **0.4** | 76.2 |
| 6 This study★ | 28.3 | 96.5 | 600 | 236 | **460** | **1.3** | 2.9 |

section should be waterproof and immersed under the seawater surface by adjusting the buoyancy module of the device. Due to the vast thermal capacity and constant temperature of seawater, the heat generated by the compressor can be removed rapidly and will not contribute to the temperature rise in the device, thus being beneficial to reduce the air flow rate and increase the condensing ratio, and then improve the device performance. As well, some novel light-weight materials should be introduced in fabricating the main body of the device to reduce the volume of the buoyancy cylinders resulting in the device occupying less space in the ship (Mohee *et al.* 2016a, 2016b, 2017; Mohee & Al-Mayah 2017a, 2017b, 2018; Mohee 2017).

### Cost of the experimental prototype

The cost of the experimental prototype detailed in Table 4 mainly includes four parts. The most expensive part is the power supply and control module, and it is composed of two lithium batteries, which are worth 425 US dollars, and others, such as two collapsible solar panels, a controller and several sensors, which are worth 294.5 dollars in total. The plastic shell, internal structures, and buoyancy cylinders cost 322.3 dollars including the materials and the manufacturing. The water generating module was designed as an entirety, and is a total of 102 dollars. The cost of the water purifying module is 28.5 dollars, including the ultrafilter and necessary pipes.

## CONCLUSIONS

To offer an alternative for supplying fresh water to people in distress in tropical seas before rescue or for garrison soldiers on a small reef, a portable solar-PV AWG (PS-AWG) with compression refrigeration cycles and lower energy consumption was designed and tested experimentally. The main principle of potable water generation is to humidify and dehumidify the air by 'natural water evaporator' and a compression refrigeration cycle, respectively. The device is composed of a water generating module, a water purifying module, a power supply and control module, and a buoyancy module.

**Table 4** | Cost of the experimental prototype

| Project | Cost ($) |
|---|---|
| Water generating module | 102 |
| Water purifying module | 28.5 |
| Power supply and control module | 719.5 |
| Buoyancy module | 322.3 |
| Total | 1,172.3 |

To test the performance of the device, an experimental prototype was fabricated and a testing platform was built. The best water production rate of 460 mL/h can be achieved when $T_{in} = 27$, $RH_{in} = 92\%$, $Q_a = 600$ m$^3$/h, with the desalination rate above 99.65%, proving itself a feasible solution as a portable desalination device. The influences of major operating parameters on the device performance, especially on the water production rate and the energy conversion coefficient, were analyzed. Increase of temperature, relative humidity, and flow rate of air flow at the inlet would improve the device performance, yet there is an upper limit of temperature. The salinity of the feed water had no influence on the performance, indicating that the salinity of the seawater is not a consideration for the application of the device. Performance comparisons were also carried out among the AWG products/prototypes available and the proposed AWG. The experimental prototype in this study performed well with higher water production rate and less energy consumption; the tested daily water production rate was more than twice the minimum quantity of the WHO drinking water standard.

The main drawback of the device is its low condensation efficiency due to large air flow rate and insufficient cooling of the compressor. The device could be further improved by designing a separate cooling system for the compressor which is independent of the air flow. An extra section can be designed at the bottom of the device, immersed under the seawater surface, in which the compressor is mounted separately. For the vast thermal capacity and constant temperature of seawater, the heat generated by the compressor can be removed rapidly and will not contribute to the inner temperature rise, which is beneficial in reducing the air flow rate and increasing the condensing ratio, and thus improving the device's performance. As well, some novel light-weight materials should be introduced in fabricating the main body of the device to reduce the volume of the buoyancy cylinders and resulting in taking up less space on the ship.

In further applications, the device can be integrated with a distress signal launcher and positioning module to shorten

rescue time. Thus, it can be employed as a small rescue platform for people in distress in tropical oceans, not only supplying potable water but also assisting in their rescue, carried on board as a precaution.

## ACKNOWLEDGEMENTS

The financial support by the National Natural Science Foundations of China (51769006) is gratefully acknowledged. Du Renze and Lu Hui have contributed equally to the work.

## REFERENCES

Abdessemed, A., Boubekeur, H., Boublai, N. & Bougriou, C. 2019 Experimental investigation of a poly-energy multi-effect still in Algeria. *Water Supply* **19**, 926–931. https://doi.org/10.2166/ws.2018.143.

Alobaid, M., Hughes, B., Calautit, J. K., O'Connor, D. & Heyes, A. 2017 A review of solar driven absorption cooling with photovoltaic thermal systems. *Renewable and Sustainable Energy Reviews* **76**, 728–742. https://doi.org/10.1016/j.rser.2017.03.081.

Anbarasu, T. & Pavithra, S. 2011 Vapour compression refrigeration system generating fresh water from humidity in the air. In: *International Conference on Sustainable Energy and Intelligent Systems (SEISCON 2011)*, Chennai, India.

Arunkumar, T., Jayaprakash, R., Denkenberger, D., Ahsan, A., Okundamiya, M. S., Kumar, S., Tanaka, H. & Aybar, H. Ş. 2012 An experimental study on a hemispherical solar still. *Desalination* **286**, 342–348. https://doi.org/10.1016/j.desal.2011.11.047.

Dashtban, M. & Tabrizi, F. F. 2011 Thermal analysis of a weir-type cascade solar still integrated with PCM storage. *Desalination* **279**, 415–422. https://doi.org/10.1016/j.desal.2011.06.044.

Esfahani, J. A., Rahbar, N. & Lavvaf, M. 2011 Utilization of thermoelectric cooling in a portable active solar still – an experimental study on winter days. *Desalination* **269**, 198–205. https://doi.org/10.1016/j.desal.2010.10.062.

Farhad, S., Alireza, N. M. & Mohammad, M. N. 2018 Thermodynamic analysis and improvement of a novel solar driven atmospheric water generator. *Energy Conversion and Management* **161**, 101–111. https://doi.org/10.1016/j.enconman.2018.01.066.

Fox, C. H., O'Hara, P. D., Bertazzon, S., Morgan, K., Underwood, F. E. & Paquet, P. C. 2016 A preliminary spatial assessment of risk: marine birds and chronic oil pollution on Canada's Pacific coast. *Science of the Total Environment* **573**, 799–809. https://doi.org/10.1016/j.scitotenv.2016.08.145.

Freire-Gormaly, M. & Bilton, A. 2017 An experimental system for characterization of membrane fouling of solar photovoltaic reverse osmosis systems under intermittent operation. *Desalination and Water Treatment* **73**, 54–63. https://doi.org/10.5004/dwt.2017.20391.

Freire-Gormaly, M. 2018 *Experimental Characterization of Membrane Fouling Under Intermittent Operation and Its Application to the Optimization of Solar Photovoltaic Powered Reverse Osmosis Drinking Water Treatment Systems*. PhD Thesis, Department of Mechanical and Industrial Engineering, University of Toronto, Canada.

Freire-Gormaly, M. & Bilton, A. 2018 Experimental quantification of the effect of intermittent operation on membrane performance of solar powered reverse osmosis desalination systems. *Desalination* **435**, 188–197. https://doi.org/10.1016/j.desal.2017.09.013.

Freire-Gormaly, M. & Bilton, A. 2019a Design of photovoltaic powered reverse osmosis desalination systems considering membrane fouling caused by intermittent operation. *Renewable Energy* **135**, 108–121. https://doi.org/10.1016/j.renene.2018.11.065.

Freire-Gormaly, M. & Bilton, A. 2019b Impact of intermittent operation on reverse osmosis membrane fouling for brackish groundwater desalination systems. *Journal of Membrane Science* **583**, 220–230. https://doi.org/10.1016/j.memsci.2019.04.010.

Goerlandt, F. & Montewka, J. 2015 A framework for risk analysis of maritime transportation systems: a case study for oil spill from tankers in a ship–ship collision. *Safety Science* **76**, 42–66. https://doi.org/10.1016/j.ssci.2015.02.009.

Joshi, V. P., Joshi, V. S., Kothari, H. A., Mahajan, M. D., Chaudhari, M. B. & Sant, K. D. 2017 Experimental investigations on a portable fresh water generator using a thermoelectric cooler. *Energy Procedia* **109**, 161–166. https://doi.org/10.1016/j.egypro.2017.03.085.

Kabeel, A. E., Abdulaziz, M. & El-Said, E. M. 2016 Solar-based atmospheric water generator utilization of a fresh water recovery: a numerical study. *International Journal of Ambient Energy* **37** (1), 68–75. https://doi.org/10.1080/01430750.2014.882864.

Kabeel, A. E., Teamah, M. A., Abdelgaied, M. & Abdel Aziz, G. B. 2017 Modified pyramid solar still with v-corrugated absorber plate and PCM as a thermal storage medium. *Journal of Cleaner Production* **161**, 881–887. https://doi.org/10.1016/j.jclepro.2017.05.195.

Li, R., Shi, Y., Alsaedi, M., Wu, M., Shi, L. & Wang, P. 2018 Hybrid hydrogel with high water vapor harvesting capacity for deployable solar-driven atmospheric water generator. *Environmental Science and Technology* **52** (19), 11367–11377. https://doi.org/10.1021/acs.est.8b02852.

Liu, S., He, W., Hu, D., Lv, S., Chen, D., Wu, X., Xu, F. & Li, S. 2017 Experimental analysis of a portable atmospheric water generator by thermoelectric cooling method. *Energy Procedia* **142**, 1609–1614. https://doi.org/10.1016/j.egypro.2017.12.538.

Madhlopa, A. & Johnstone, C. 2009 Numerical study of a passive solar still with separate condenser. *Renewable Energy* **34**, 1668–1677. https://doi.org/10.1016/j.renene.2008.12.032.

Mohee, F. M. 2017 *Development, Analysis and Testing of Innovative Mechanical Prestressing Anchors for CFRP Plates for Structural Rehabilitation and Retrofitting*. PhD Thesis,

University of Waterloo (UWSpace), Canada. http://hdl.handle.net/10012/11207

Mohee, F. M. & Al-Mayah, A. 2017a Development of an innovative prestressing CFRP plate anchor: numerical modelling and parametric study. *Composite Structures* **177**, 1–12. https://doi.org/10.1016/j.compstruct.2016.12.039.

Mohee, F. M. & Al-Mayah, A. 2017b Effect of modulus of elasticity and thickness of the CFRP plate on the performance of a novel anchor for structural retrofitting and rehabilitation applications. *Engineering Structures* **153**, 302–316. https://doi.org/10.1016/j.engstruct.2017.09.057.

Mohee, F. M. & Al-Mayah, A. 2018 Effect of barrel, wedge material and thickness on composite plate anchor performance through analytical, finite element, experimental and 3D prototype investigations. *Engineering Structures* **175**, 138–154. https://doi.org/10.1016/j.engstruct.2018.08.003.

Mohee, F. M., Al-Mayah, A. & Plumtree, A. 2016a Anchors for CFRP plates: state-of-the-art review and future potential. *Composites Part B: Engineering* **90**, 432–442. https://doi.org/10.1016/j.compositesb.2016.01.011.

Mohee, F., Al-Mayah, A. & Plumtree, A. 2016b Friction characteristics of CFRP plates in contact with copper plates under high contact pressure. *Journal of Composites for Construction* **4016022**. https://doi.org/10.1061/(ASCE)CC.1943-5614.0000673.

Mohee, F. M., Al-Mayah, A. & Plumtree, A. 2017 Development of a novel prestressing anchor for CFRP plates: experimental investigations. *Composite Structures* **176**, 20–32. https://doi.org/10.1016/j.compstruct.2017.05.011.

Murugavel, K. K., Sivakumar, S., Riaz Ahamed, J., Chockalingam, K. K. S. K. & Srithar, K. 2010 Single basin double slope solar still with minimum basin depth and energy storing materials. *Apply Energy* **87**, 514–523. https://doi.org/10.1016/j.apenergy.2009.07.023.

Mutasher, S. A., Mir-Nasiri, N., Wong, S. Y., Ngoo, K. C. & Wong, L. Y. 2010 Improving a conventional greenhouse solar still using sun tracking system to increase clean water yield. *Desalination and Water Treatment* **24**, 140–149. https://doi.org/10.5004/dwt.2010.1473.

Nagarajan, P. K., Vijayakumar, D., Paulson, V., Chitharthan, R. K., Ramanarayanan, Y. N. & Sathyamurthy, R. 2014 Performance evaluation of triangular pyramid solar still for enhancing productivity of fresh water. *Research Journal of Pharmaceutical Biological and Chemical Sciences* **5**, 764–771.

Niewenhuis, B., Shepperly, C., Beek, R. V. & Kooten, E. V. 2012 *Water Generator Water From Air Using Liquid Desiccant Method*. Design report. Calvin College, Grand Rapids, MI, USA.

Omara, Z. M., Kabeel, A. E. & Abdullah, A. S. 2017 A review of solar still performance with reflectors. *Renewable & Sustainable Energy Reviews* **68**, 638–649. https://doi.org/10.1016/j.rser.2016.10.031.

Pontious, K., Weidner, B., Guerin, N., Dates, A., Pierrakos, O. & Altaii, K. 2016 Design of an atmospheric water generator: harvesting water out of thin air. In: *IEEE Systems and Information Engineering Design Symposium*, Charlottesville, VA, USA.

Praene, J. P., Marc, O., Lucas, F. & Miranville, F. 2011 Simulation and experimental investigation of solar absorption cooling system in Reunion Island. *Applied Energy* **88** (3), 831–839. https://doi.org/10.1016/j.apenergy.2010.09.016.

Rahbar, N. & Esfahani, J. A. 2012 Experimental study of a novel portable solar still by utilizing the heatpipe and thermoelectric module. *Desalination* **284**, 55–61. https://doi.org/10.1016/j.desal.2011.08.036.

Rahbar, N., Esfahani, J. A. & Asadi, A. 2016 An experimental investigation on productivity and performance of a new improved design portable asymmetrical solar still utilizing thermoelectric modules. *Energy Conversion and Management* **118**, 55–62. https://doi.org/10.1016/j.enconman.2016.03.052.

Rajaseenivasan, T., Elango, T. & Murugavel, K. K. 2013 Comparative study of double basin and single basin solar stills. *Desalination* **309**, 27–31. https://doi.org/10.1016/j.desal.2012.09.014.

Sathyamurthy, R., Kennady, H. J., Nagarajan, P. K. & Ahsan, A. 2014 Erratum to 'Factors affecting the performance of triangular pyramid solar still'. *Desalination* **344**, 383–390. https://doi.org/10.1016/j.desal.2014.05.042.

Sathyamurthy, R., El-Agouz, S. A. & Dharmaraj, V. 2015 Experimental analysis of a portable solar still with evaporation and condensation chambers. *Desalination* **347**, 180–185. https://doi.org/10.1016/j.desal.2015.04.012.

Sheeba, K. N., Prakash, P. & Jaisankar, S. 2015 Performance evaluation of a flat plate collector coupled solar still system. *Energy Sources Part A-Recovery Utilization and Environmental Effects* **37**, 291–298. https://doi.org/10.1080/15567036.2011.585379.

Singh, D. B. & Tiwari, G. N. 2017 Energy, exergy and cost analyses of N identical evacuated tubular collectors integrated basin type solar stills: a comparative study. *Solar Energy* **155**, 829–846. https://doi.org/10.1016/j.solener.2017.07.018.

Størkersen, K. V., Antonsen, S. & Kongsvik, T. 2017 One size fits all? safety management regulation of ship accidents and personal injuries. *Journal of Risk Research* **20** (9), 1154–1172. https://doi.org/10.1080/13669877.2016.1147487.

Vián, J. G., Astrain, D. & Domínguez, M. 2002 Numerical modelling and a design of a thermoelectric dehumidifier. *Applied Thermal Engineering* **22** (4), 407–422. https://doi.org/10.1016/S1359-4311(01)00102-8.

Wassouf, P., Peska, T., Singh, R. & Akbarzadeh, A. 2011 Novel and low cost designs of portable solar stills. *Desalination* **276**, 294–302. https://doi.org/10.1016/j.desal.2011.03.069.

Yıldırım, C., Soylu, S. K., Atmaca, I. & Solmus, I. 2014 Experimental investigation of a portable desalination unit configured by a thermoelectric cooler. *Energy Conversion and Management* **85**, 140–145. https://doi.org/10.1016/j.enconman.2014.05.071.

First received 8 July 2019; accepted in revised form 28 December 2019. Available online 20 February 2020